Optical Materials 32 (2010) 652–656

Contents lists available at ScienceDirect

Optical Materials

journal homepage: www.elsevier.com/locate/optmat

The effect of hydrostatic pressure on the combustion synthesis of Y_2O_3:Bi nanophosphor

L.G. Jacobsohn [a,b,1], B.C. Tappan [a], S.C. Tornga [a], M.W. Blair [a,*], E.P. Luther [a], B.A. Mason [a], B.L. Bennett [a], R.E. Muenchausen [a]

[a] Los Alamos National Laboratory, Los Alamos, NM 87544, United States
[b] School of Materials Science and Engineering, and Center for Optical Materials Science and Engineering Technologies, Clemson University, Anderson, SC 29625, United States

ARTICLE INFO

Article history:
Received 1 July 2009
Received in revised form 7 December 2009
Accepted 11 January 2010

Keywords:
Photoluminescence
SCS
Y_2O_3:Bi
Thermoluminescence
Luminescence lifetime

ABSTRACT

The effects of pressurized Ar environments during the solution combustion synthesis (SCS) of Y_2O_3:Bi nanophosphor were investigated. Three fuels were used urea, glycine and hexamethylenetetramine (HMT) and the nanopowders were characterized by X-ray diffraction, scanning electron microscopy, photoluminescence, fluorescence lifetime, and thermoluminescence measurements. The dominant crystallographic phase was cubic, with crystallite size being insensitive to the hydrostatic pressure but increasing for fuels with higher heat of combustion. At least for nanopowders obtained using fuels with higher heats of combustion, higher Ar hydrostatic pressures lead to lower photoluminescence output. Fluorescence lifetime measurements on HMT-prepared samples yielded lifetimes of 330 and 900 ns for Bi^{3+} ions in S_6 and C_2 sites, respectively, and no variation in these values was observed for hydrostatic pressures from 0.1 to 9.7 MPa. Shorter lifetime values than reported for conventional SCS are likely related to higher concentration of quenching defects. In agreement with these results, thermoluminescence measurements showed that higher concentrations of electronic traps are present in samples synthesized under higher pressures.

1. Introduction

The emergence of nanoscience opened up a new dimension in Materials Science, where modification of properties and functionalities by means of reduced dimensionality effects are explored to achieve unique properties and more efficient devices. Many techniques have been used to produce nanomaterials [1], one among them is solution combustion synthesis (SCS). This technique was first used in the late 80's/early 90's to produce nanopowders of oxides [2,3]. To date, numerous simple and complex oxides have been synthesized, including aluminates, silicates, rare earth oxides, and nanocomposites. In particular, this technique has been used to produce nanophosphors, including complex Ce-doped oxyorthosilicates [4–7].

SCS is a robust, inexpensive synthesis method with high production yield of nanocrystalline oxide powders that can be easily scaled-up for large production. It is based on exothermic redox reactions that undergo self-sustaining self-propagating combustion. Mixtures of metal nitrates and a fuel ignite and sustain combustion under furnace heating, and the chemical energy from the exothermic reaction, heats the precursor mixture to high temperatures promoting chemical bonding, agglomeration and crystallization. The final product is a nanocrystalline ceramic foam that can be easily ground into powder. Despite the advantages of the SCS method, this process is stochastic in nature and not well understood. Currently, it is not possible to properly model the combustion process or to predict the characteristics of materials produced by SCS *a priori*, simply based on combustion conditions. On the other hand, many parameters like fuel type, fuel/nitrate ratio, water content, etc., are empirically known to affect the nanopowder characteristics, including their morphology and crystallite size [3,4,8–12].

Bi^{3+} ions are commonly used to activate materials and serve as a useful probe of host characteristics as their luminescence is known to be highly sensitive to the coordination of the activator site [20,26]. Recently, we reported the correlation of the heat of combustion of the fuel with the average particle size and crystallinity of Y_2O_3:Bi nanopowders [13]. The effects of high-pressure compression, in the 60–120 MPa range, during combustion synthesis have been used to promote densification [14], *e.g.*, in α-Al_2O_3 [15] and $MgAl_2O_4$–TiAl composites [16]. On the other hand, besides McKittrick et al. who reported the effects of 1–5 MPa Ar hydrostatic pressures on the crystalline phase of alumina powders [17,18], the low pressures effects of ~1–10 MPa are essentially

* Corresponding author. Tel.: +1 505 667 7981; fax: +1 505 665 3866.
E-mail address: mblair@lanl.gov (M.W. Blair).
[1] Present address.

0925-3467/$ - see front matter © 2010 Elsevier B.V. All rights reserved.
doi:10.1016/j.optmat.2010.01.019

unexplored. In this work, we utilize the coordination environment sensitivity of the Bi^{3+} ion to investigate the effects of hydrostatic pressure during the synthesis of Y_2O_3:Bi nanophosphor on its morphology, structure and luminescent properties. Whenever possible, the results are compared to those obtained from samples produced by conventional SCS, *i.e.*, SCS is carried out in ambient pressure and atmosphere, and with data on Y_2O_3:Bi produced by solid state reaction [19,20].

2. Experimental procedures

Precursor solid mixtures were produced using three different organic fuels: urea, glycine, and HMT. To obtain $Y(NO_3)_3$, 3 g of Y_2O_3 nanopowder (Alfa Aesar 99.9%, 25–50 nm) was dissolved in an excess of nitric acid (7 mL, Baker, Huey HNO_3, 65 wt%). The amount of $Bi(NO_3)_3{\cdot}XH_2O$ (Alfa Aesar, Puratronics, 5 N), with *X* assumed to be 6, was calculated with respect to the mass of Y_2O_3 per crucible to yield 1 mol% (67 mg of $Bi(NO_3)_3{\cdot}6H2O$ corresponds to 1 mol% doping). After this gentle exothermic reaction cooled, a fixed amount of fuel, 4.32 g of glycine (Fisher, reagent grade), 5.2 g of urea (Baker analyzed reagent grade), or 2.1 g of HMT (Fisher, certified A.C.S.), were added to each crucible and thoroughly mixed. The amount of fuel was calculated assuming full combustion of the starting material [13]. Prior to combustion, the mixture was dried in a vacuum oven at 115 °C for 24 h and then pressed into pellets. Combustion synthesis was carried out by means of local ignition using a nickel–chromium wire to ignite the pelletized precursor solid mixture in a 2 l volume chamber with controlled Ar atmospheres (Fig. 1(A)) [21], as well as by heating the whole pellet in a muffle furnace set at 600 °C in ambient pressure and atmosphere. The latter is referred to as "conventional" SCS [13] that uses a Büchner funnel to contain the produced foam in the furnace shown in Fig. 1(B).

Structural and morphological characterization was carried out by X-ray diffraction (XRD) using a Siemens D5000 X-ray diffractometer with $Cu_{K\alpha}$ radiation, and scanning electron microscopy (SEM) using a JEOL7000 field emission microscope with a Schottky type (T-FE) emitter, respectively.

Photoluminescence excitation (PLE), emission (PL) and fluorescence lifetime measurements were obtained in ambient conditions using a Photon Technology International TimeMaster™ fluorimeter.

Thermoluminescence (TL) experiments were carried out on a Risø TL/OSL DA-15 automated system. The samples were affixed to stainless steel disks using silicone spray and irradiations were performed with an on-board $^{90}Sr/^{90}Y$ β irradiation source delivering approximately 0.13 Gy/s. The samples were heated at a rate of 1 °C/s and light detection was accomplished via a photomultiplier tube with bialkali photocathode (Thorn-EMI 9235QA) combined with a Schott BG39 filter (350–600 nm).

3. Results and discussion

In this work, Y_2O_3:Bi nanopowders were produced by conventional SCS and by combustion under isostatic Ar pressures using three fuels: urea, glycine, and HMT. Fig. 1A illustrates the synthesis of Y_2O_3:Bi nanophosphor under controlled Ar pressure, in this case 9.6 MPa of Ar and using glycine as fuel. The image was extracted using a high-speed image recording system and shows the self-propagating combustion front as the bright region on top of the pellet, and the nanocrystalline foam expanding outwards. In conventional SCS, the fuel–reactant mixture simultaneously ignites as a whole upon heating, concomitant with the generation of gases and flames as illustrated in Fig. 1B. In both cases, a nanocrystalline ceramic foam that can be easily ground to powder is formed. The

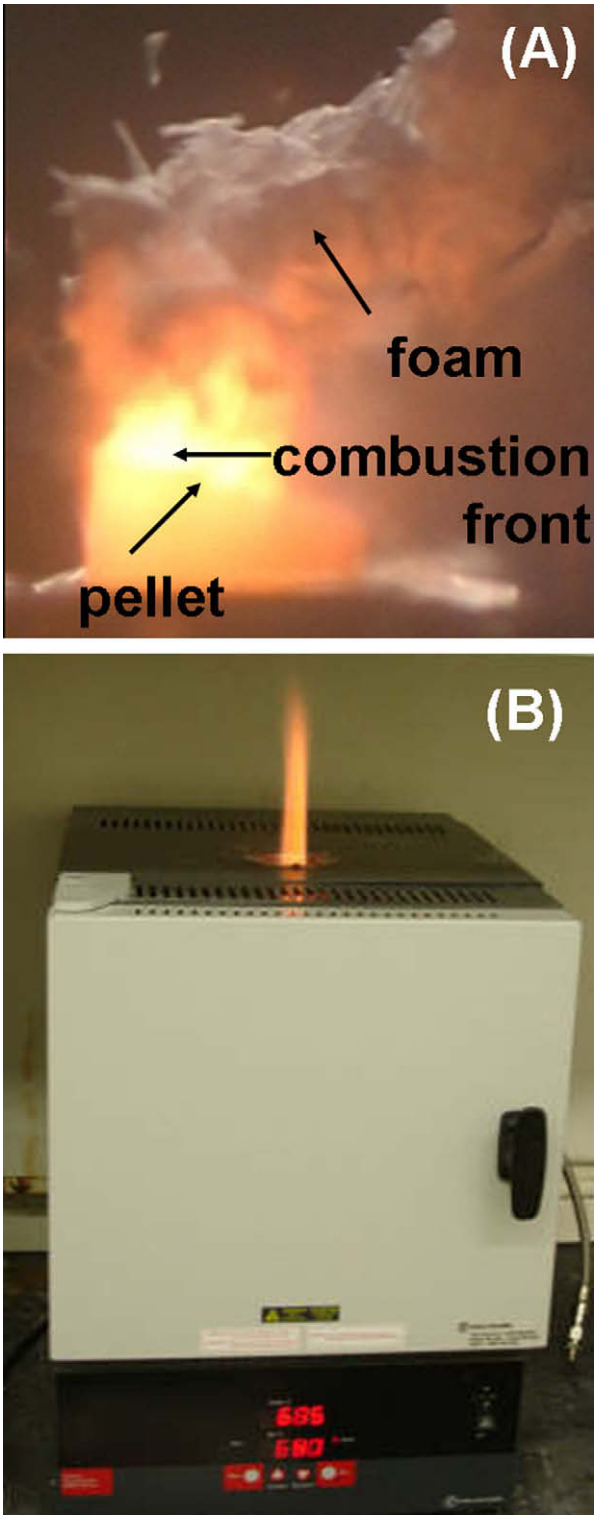

Fig. 1. Combustion processes in: (A) 9.6 MPa Ar atmosphere; glycine as fuel (B) conventional SCS.

effects of the hydrostatic pressure on the morphology of the nanopowders were characterized by SEM in secondary electron mode to enhance surface features, and selected results are presented in Fig. 2 for nanopowders synthesized using HMT. Images of nanopowders obtained with Ar pressure ranging from 1 atmosphere (0.1 MPa) to 9.7 MPa show the presence of fine grains with typical dimensions of a fraction of a micron fused together. Only the sam-

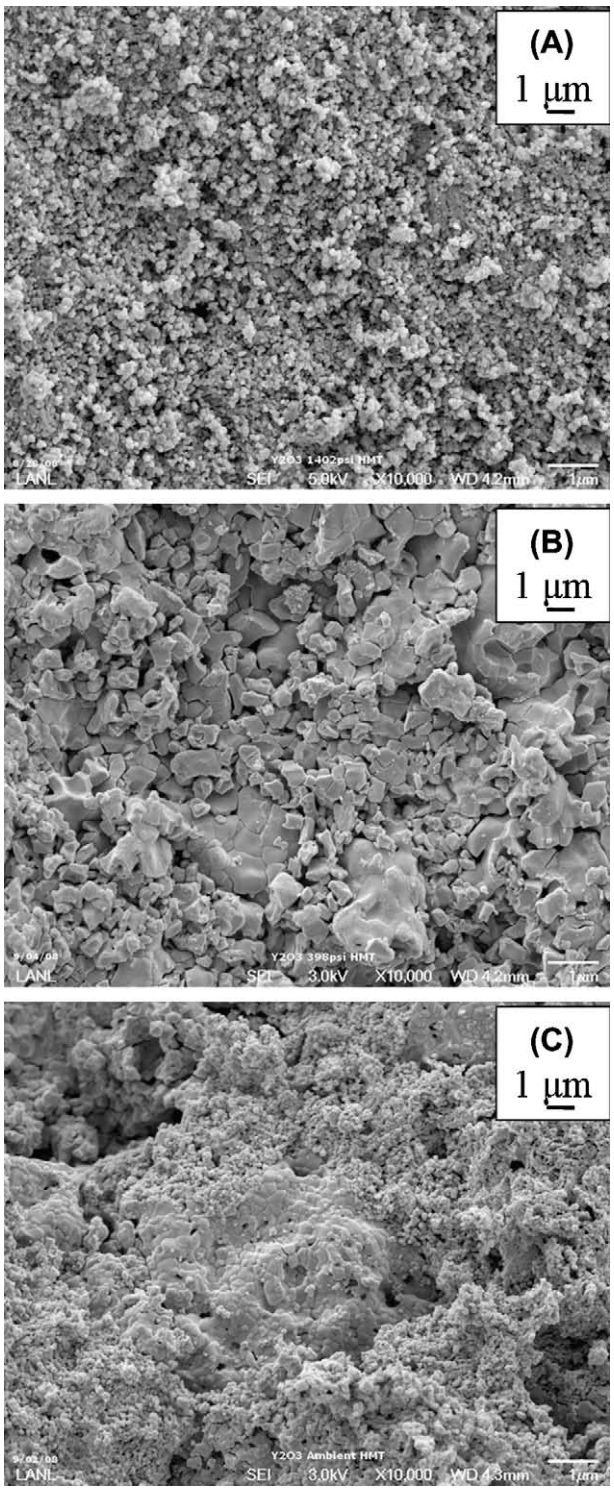

Fig. 2. SEM images of nanopowders produced using HMT as fuel at different Ar pressures: (A) 9.7, (B) 2.7, and (C) 0.1 MPa.

ple synthesized at the highest pressure presents morphological homogeneity from low to high magnification, with grains sizing ~0.1 μm (Fig. 2A). For samples synthesized at 0.1 and 2.7 MPa, the morphology is less homogeneous with larger grains (~0.3 μm) embedded in regions composed of much smaller grains (<0.1 μm), as seen in Fig. 2B and C.

The structure of nanopowders was characterized by XRD. For urea, a single crystallographic cubic Y_2O_3 phase (PDF41–1105) was obtained for all Ar pressures. For glycine and HMT, while diffraction is dominated by the cubic Y_2O_3 phase, a weak diffraction peak at ~27° was noticed, indicating the presence of an unidentified secondary phase which could be another yttria or Bi oxide phase. These results are illustrated in Fig. 3 for the highest Ar pressure for each fuel. For conventional SCS, single crystallographic cubic Y_2O_3 phase was obtained using glycine and HMT, while urea yielded a Bi oxide phase in addition to the cubic Y_2O_3 phase [13]. Crystallite sizes were estimated using the Debye–Scherrer method and the width of peaks at 20.5°, 29.2° and 33.8° corresponds to the (2 1 1), (2 2 2), and (4 0 0) crystallographic planes, respectively. These results are presented in Table 1, where it is possible to infer that the increase of the heat of combustion of the fuel from urea (636 kJ/mol [22]) to glycine (980 kJ/mol [22]) to HMT (4215 kJ/mol [22]) leads to an increase in our stoichiometric reaction combustion energy (55 kJ, 56.4 kJ and 63 kJ respectively) which corresponds with a small increase of the average crystallite size, from 26 to 37 nm. However, changes in the hydrostatic pressure have no significant effect on the crystallite size. The same size trend with fuel was observed with conventional SCS, though a much broader range of crystallite sizes, from 9 to 29 nm, was obtained.

Y_2O_3 has a bcc structure with Ia3 symmetry where there are two 6-coordinated non-equivalent cation sites. These sites correspond to atomic configurations where two oxygen vacancies are

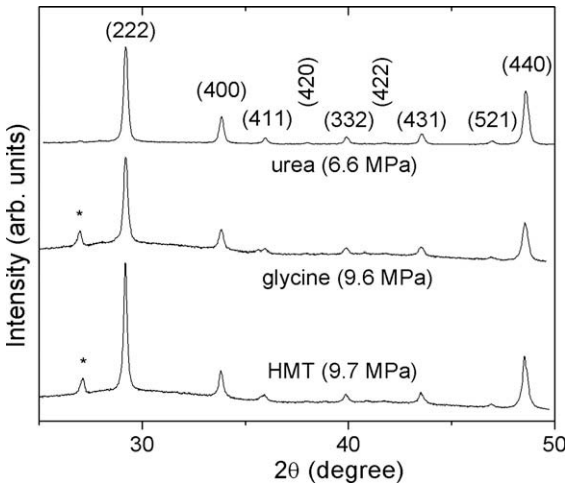

Fig. 3. XRD results of nanopowders prepared at highest Ar pressures for each fuel, respectively. The star marks the peak of the impurity phase.

Table 1
Crystallite size determined by the Debye–Scherrer method for samples prepared with different fuels at controlled Ar atmospheres or in ambient pressure and atmosphere (conventional SCS; *).

Fuel	Ar pressure (MPa)	Size (nm)			Average rounded size (nm)
		20.5° (211)	29.2° (222)	33.8° (400)	
Urea	2.8	28.1	27.3	22.8	26
	4.9	25.5	26.0	25.2	26
	6.6	29.5	29.3	28.5	29
	0.1*	8.9	–	–	9
Glycine	3.5	29.4	29.7	28.9	29
	6.9	32.2	31.6	30.8	32
	9.6	–	31.3	29.8	31
	0.1*	13.5	12.4	13.1	13
HMT	0.1	–	38.1	36.4	37
	2.7	–	37.0	37.7	37
	9.7	–	37.6	34.0	36
	0.1*	30.4	29.3	27.6	29

located on a cube (S_6) or face (C_2) diagonal. Their occupancies are 8 and 24, respectively, out of the 32 sites that comprise the unit cell of Y_2O_3. The S_6 sites present inversion symmetry and are rather symmetrical, while the C_2 sites are rather irregular since there are more atoms on one side of the luminescent center than on the other. These structural differences manifest themselves in different local crystalline fields experienced by the Bi^{3+} ions which affect their luminescent behavior. Two emission bands have been observed in Y_2O_3:Bi^{3+} at about 408 and 505 and assigned to S_6 and C_2 sites, respectively [19,20]. However, defects can perturb the local site symmetry of the luminescent center and quench luminescence. Measurements of fluorescence lifetime are sensitive to the presence of quenching defects, with a decrease in the measured lifetime corresponding to higher concentrations of quenching defects. Fluorescence lifetime τ, can be written as: $1/\tau = 1/\tau_{radiative} + 1/\tau_{quenched}$, where $1/\tau_{radiative}$ corresponds to the probability for radiative emission, and $1/\tau_{quenched}$ corresponds to the probability of non-radiative decay due to defect quenching [23]. Fluorescence lifetime measurements of nanopowders prepared using HMT as fuel were carried out for both crystallographic sites aiming to identify the effect of hydrostatic pressure on the concentration of quenching defects. Lifetime values were determined by means of an iterative procedure based on the Marquardt algorithm where the experimental data are compared to the convolution between the instrumental response and the single exponential model for the fluorescence decay. The final values of 330 (+2%) and 900 (+5%) ns for Bi^{3+} ions in S_6 and C_2 sites, respectively, remained the same within a few % variation, as indicated, for Ar pressures from 0.1 to 9.7 MPa. On the other hand, Y_2O_3:Bi prepared by conventional SCS using HMT as fuel and annealed at 1000 °C for 1 h to eliminate organic residues yielded values of 450 and 1190 ns for Bi^{3+} ions in S_6 and C_2 sites, respectively, while fluorescence lifetime measurements of the C_2 site in bulk Y_2O_3:Bi prepared by solid state reaction yielded values of 500/550 ns [19,20] (to the best of our knowledge, there are no measurements for S_6 sites in bulk Y_2O_3:Bi). These results show that conventional SCS produces materials with lower quenching defect concentration than combustion in propagation mode in controlled Ar atmospheres and solid state reaction. This is in agreement with previous results on Ce-doped oxyorthosilicates produced by conventional SCS that presented concentrations of thermoluminescent defects ~2000 times lower than bulk crystals produced by the Czochralski method [24].

Fig. 4 presents PLE and PL for Bi^{3+} in S_6 sites for nanopowders as a function of the hydrostatic Ar pressure. PLE spectra were obtained while monitoring emission at 408 nm, and PL spectra were obtained under excitation at 373 nm. The Stokes shift for the bulk and nanomaterials were all similar, around 0.3 eV. More importantly, PL intensity for all the synthesis conditions is presented in Fig. 5 where a clear monotonic decrease for higher pressures can be observed. For the fuels with the higher heats of combustion, glycine and HMT, the PL intensities decreased by factors of approximately 2 and 5 respectively for the highest pressure. In the case of urea, while being the brightest material, a clear trend with pressure was not found, with all values being scattered within 25% of the average intensity value. It should also be noted that PL intensity is inversely related to the heat of combustion (e.g., urea shows the highest PL intensity) which agrees with the previous findings in Jacobsohn et al. [13] which found that PL intensity varies directly with crystallinity.

TL behavior was investigated for nanopowders prepared using HMT as fuel to provide insight on electronic traps that might induce quenching, and results are shown in Fig. 6 as a function of Ar hydrostatic pressure and irradiation dose. The results were normalized by sample mass to allow for direct comparison between the plots. Three main peaks located around 80, 200 and 350 °C were consistently observed, though their relative intensities changed for different hydrostatic pressures. Though the peak temperatures are dependent on the measurements conditions and thus have limited physical meaning, we will refer to each peak by their peak temperature for simplicity. In all samples, the 200 °C peak is the most intense one. It remains constant for pressures up to 2.7 MPa and then increases approximately 50% for 9.7 MPa. The analysis of the peak positions shows that the low temperature peak (80 °C) does not shift with irradiation dose suggesting a first order TL relaxation mechanism, while the 200 °C peak shifts to lower temperatures for doses above ~12 Gy, and the 350 °C peak rapidly shifts to higher temperatures for increasing irradiation doses. On the other hand, Y_2O_3:Bi samples prepared by conventional SCS using HMT as fuel and measured in the same conditions present peaks at 110, 138 and 250 °C [13]. Further, comparison with results from bulk undoped Y_2O_3 measured with a heating rate of 0.32 °C/s, where only two peaks at 115 and 190 °C were observed [25], and with conventional SCS-prepared undoped Y_2O_3 measured at 5 °C/s that shows two peaks at 111 and 172 °C suggests that the incorporation of Bi^{3+} ions is responsible for the creation of additional

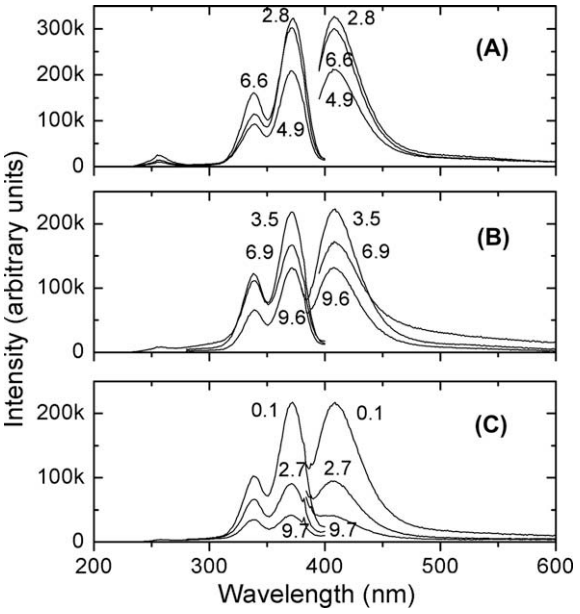

Fig. 4. PLE and PL spectra of Bi^{3+} in S_6 sites for various hydrostatic synthesis pressures as labeled (in MPa) for different fuels: (A) urea, (B) glycine, and (C) HMT.

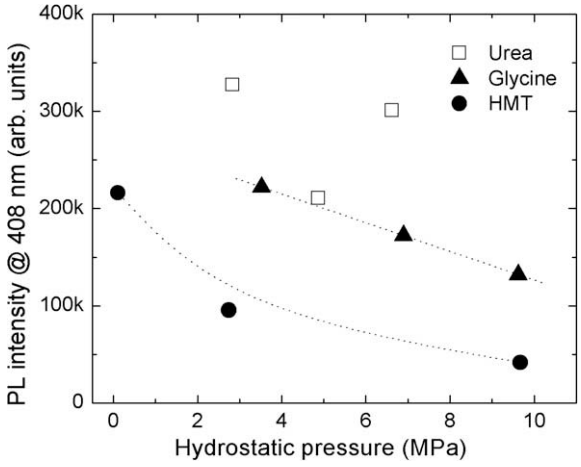

Fig. 5. Absolute PL intensity of band centered at 408 nm for different fuels as a function of hydrostatic pressure.

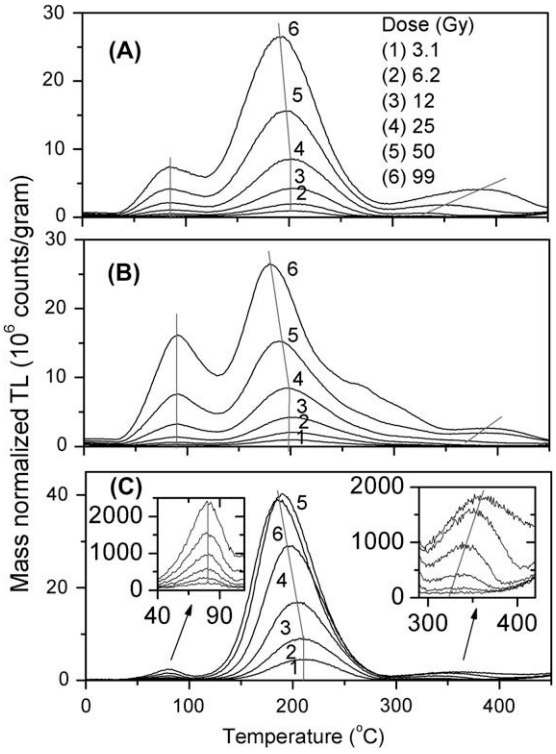

Fig. 6. TL results for HMT-prepared Y_2O_3:Bi nanophosphor using different Ar pressures: (A) 0.1 MPa, (B) 2.7 MPa, and (C) 9.7 MPa. The gray lines are guides to the eye only.

electron traps. Interestingly, some TL peaks occur at similar temperatures (*e.g.*, 110, 111 and 115 °C; 190 and 200 °C) and thus may well correspond to the same type of trap having slightly different energy depths below the conduction band due to structural disorder. These results reflect the non-stochastic nature of the combustion process in creating defects with varying concentrations for different synthesis conditions. Further work is necessary to fully analyze the characteristics and nature of these defects. More importantly, the TL results showed that higher concentrations of electron trapping centers are produced by combustion in propagation mode and Ar atmospheres than by conventional SCS. Although traps in the TL process cannot be directly linked to the quenching defects involved in the PL process, the fluorescence lifetime and TL measurements support each other in that more defects are observed in materials produced in propagation mode than in controlled Ar atmospheres.

4. Summary and conclusions

In this work, the effects of Ar hydrostatic pressure on the morphology, crystallite size, photoluminescence, fluorescence lifetime and thermoluminescence of Y_2O_3:Bi nanophosphor were investigated and compared to results obtained from materials prepared by conventional SCS and solid state reaction. It was found that controlled Ar atmospheres have little effect on the crystallite size though higher pressures tend to produce finer grains. Increase in pressure did significantly reduce PL intensity, at least for nanopowders obtained using fuels with higher heats of combustion. Additionally, the observation of shorter fluorescence lifetimes and higher TL signals for synthesis in propagation mode in controlled Ar atmospheres when compared to conventional SCS suggests the production of higher concentrations of quenching and trapping defects, respectively.

Acknowledgements

The authors would like to thank E.L. Roemer for conducting SEM measurements. This work was partially funded by the Office of Basic Energy Sciences of the Department of Energy, as well as the LANL/LDRD Program.

References

[1] B.L. Cushing, V.L. Kolesnichenko, C.J. O'Connor, Chem. Rev. 104 (2004) 3893.
[2] J.J. Kingsley, K.C. Patil, Mater. Lett. 6 (1988) 427.
[3] L.A. Chick, L.R. Pederson, G.D. Maupin, J.L. Bates, L.E. Thomas, G.J. Exarhos, Mater. Lett. 10 (1990) 6.
[4] K.C. Patil, S.T. Aruna, T. Mimani, Curr. Opin. Solid State Mater. Sci. 6 (2002) 507.
[5] S. Ekambaram, K.C. Patil, M. Maaza, J. Alloys Compd. 393 (2005) 81.
[6] V.B. Bhatkar, S.K. Omanwar, S.V. Moharil, Opt. Mater. 29 (2007) 1066.
[7] R.E. Muenchausen, E.A. McKigney, L.G. Jacobsohn, M.W. Blair, B.L. Bennett, D.W. Cooke, IEEE Trans. Nucl. Sci. 55 (2008) 1532.
[8] Y. Zhang, G.C. Stangle, J. Mater. Res. 9 (1994) 1997.
[9] J.J. Moore, H.J. Feng, Prog. Mater. Sci. 39 (1995) 243.
[10] E.J. Bosze, J. McKittrick, G.A. Hirata, Mater. Sci. Eng., B 97 (2003) 265.
[11] J. McKittrick, L.E. Shea, C.F. Bacalski, E.J. Bosze, Displays 19 (1999) 169.
[12] R. Ianos, I. Lazau, C. Pacurariu, P. Barvinschi, Eur. J. Inorg. Chem. 6 (2008) 931.
[13] L.G. Jacobsohn, M.W. Blair, S.C. Tornga, L.O. Brown, B.L. Bennett, R.E. Muenchausen, J. Appl. Phys. 104 (2008) 124303.
[14] J.J. Moore, H.J. Feng, Prog. Mater. Sci. 39 (1995) 275.
[15] F. Meng, Z. Fu, J. Zhang, H. Wang, W. Wang, Y. Wang, Q. Zhang, J. Am. Ceram. Soc. 90 (2007) 1262.
[16] D. Horvitz, I. Gotman, Acta Mater. 50 (2002) 1961.
[17] O. Ozuna, G.A. Hirata, J. McKittrick, J. Phys.: Condens. Matter 16 (2004) 2585.
[18] O. Ozuna, G.A. Hirata, J. McKittrick, Appl. Phys. Lett. 84 (2004) 1296.
[19] S.Z. Toma, D.T. Palumbo, J. Electr, Chem, Soc.: Solid State Sci. 117 (1970) 236.
[20] G. Boulon, J. Physique 32 (1971) 333.
[21] B.C. Tappan, M.H. Huynh, M.A. Hiskey, D.E. Chavez, E.P. Luther, J.T. Mang, S.F. Son, J. Am. Chem. Soc. 128 (2006) 6589.
[22] R.C. Weast (Ed.), CRC Handbook of Chemistry and Physics, 60th ed., CRC Press, Boca Raton, USA, 1980, pp. D-283.
[23] B. Henderson, G.F. Imbusch, In Optical Spectroscopy of Inorganic Solids, Oxford University Press, Oxford, UK, 1989. pp.166-247.
[24] D.W. Cooke, M.W. Blair, J.F. Smith, B.L. Bennett, L.G. Jacobsohn, E.A. McKigney, R.E. Muenchausen, IEEE Trans. Nucl. Sci. 55 (2008) 1118.
[25] M.S. Jahan, D.W. Cooke, W.L. Hults, J.L. Smith, B.L. Bennett, M.A. Maez, J. Lumin. 47 (1990) 85.
[26] G. Blasse, A. Bril, J. Chem. Phys. 48 (1968) 217.